

Wet to dry crossover and a flow vortex-lattice in active nematics

Amin Doostmohammadi¹, Michael Adamer¹, Sumesh P. Thampi¹, & Julia M. Yeomans¹

¹The Rudolf Peierls Centre for Theoretical Physics, 1 Keble Road, Oxford, OX1 3NP, UK

Active systems, from bacterial suspensions to vibrated granular matter, are continuously driven out of equilibrium by local injection of energy from their constituent elements. The energy input leads to exotic behaviour such as collective motion¹⁻³, pattern formation⁴⁻⁶, topological defects⁷⁻⁹ and active turbulence^{10,11}, but theories that link the different manifestations of activity across systems and length scales are lacking. Here we unify two different classes of active matter by using friction as a control parameter to interpolate between wet active systems, whose behaviour is dominated by hydrodynamics, and dry active matter where any flow is screened. At the wet-dry crossover, we find a novel lattice of flow vortices interleaved with an ordered network of topological defects which arises from the competition between friction and viscous dissipation. Our results contribute to understanding the physics of matter operating out-of-equilibrium, with its potential in the design of active micro- and nano-machines.

Active systems where hydrodynamic interactions are key, such as suspensions of swimming bacteria, are referred to as *wet*. The energy input to such systems is dissipated by the viscosity of the fluid. However, in many active materials there are alternative forms of dissipation, such as frictional interactions between the active particles¹² or with a substrate¹³.

In the limit where the frictional damping dominates, it screens out any velocity fields that are generated by the activity. For instance, confluent cells that are confined to layers¹⁴, the Vicsek model for migrating animal herds¹⁵, and assemblies of vibrated granular rods¹⁶ lack long-range hydrodynamic interactions and are classified as *dry* active materials. In general, a given active material will fall between these limits with the relative magnitudes of frictional and dissipative damping controlling its position on the wet-dry spectrum.

The behaviour of dry and wet active nematics is summarised pictorially at the right- and left-hand sides of Fig. 1. In the absence of momentum conservation, dry active matter is commonly described in terms of the concentration of active components and their orientational order^{17–19}. The existence of any curvature in the orientational order induces an instability that leads to the formation of bands of concentration^{18,19}. The concentration bands are, however, always unstable and eventually break into filaments that, in turn, coalesce and form new bands. The process is repeated and a chaotic regime is established²⁰.

Introducing hydrodynamics leads to extra complexity due to the coupling of the density and orientational order of active particles to the fluid flow, and distinct dynamical features are manifest in the models of wet active nematics. In particular, there is a hydrodynamic instability of nematic regions which leads to the formation of *walls*, lines of high distortions in the director field, where elastic energy is stored. The walls are continuously broken up by the creation and annihilation of topological defects, a process that gives rise once again to unstable nematic regions. The formation and removal of the walls is maintained by the active forcing, and a state termed active turbulence is established, characterised by a chaotic velocity field with regions of high vorticity^{8,21,22}.

We build upon the nematohydrodynamic equations of liquid crystals to describe a natural route from wet to dry active nematics. The variables needed to describe the hy-

hydrodynamics of a wet active nematic are ϕ the relative concentration of active and passive particles, ρ the total density, \mathbf{u} the velocity vector, and $\mathbf{Q} = \frac{q}{2}(\mathbf{nn} - \mathbf{I}/3)$, which is the nematic tensor, with q the magnitude of the orientational order, \mathbf{n} the director, and \mathbf{I} the identity tensor. The four coupled continuum equations describing the time evolution of these quantities are^{23,24}

$$\partial_t \phi + \partial_i (u_i \phi) = \Gamma_\phi \nabla^2 \mu, \quad (1)$$

$$(\partial_t + u_k \partial_k) Q_{ij} - S_{ij} = \Gamma_Q H_{ij}, \quad (2)$$

$$\partial_t \rho + \partial_i (\rho u_i) = 0, \quad (3)$$

$$\rho (\partial_t + u_k \partial_k) u_i = \partial_j \Pi_{ij} - \gamma u_i, \quad (4)$$

where the mobility and the rotational diffusivity are denoted by Γ_ϕ and Γ_Q , respectively. The co-rotation term S_{ij} accounts for the response of the orientational order to the flow gradients and the chemical potential μ and molecular field H_{ij} represent the relaxation of the orientational order and the concentration to equilibrium (see the Supplementary Information for details).

The terms on the lhs of equation (4) are the usual terms in the Navier-Stokes equation describing the inertia of the fluid. These are small at low Reynolds number, the limit relevant to active particles on the micron-scale or smaller. Contributions to the stress tensor, Π_{ij} , are the viscous dissipation, elastic stresses which encode mechanical forces on the fluid due to the relaxational motion of the active entities and, of primary relevance to our current argument, the active stress $\Pi_{ij}^{active} = -\zeta Q_{ij}$, which is proportional to the orientational order parameter and distinguishes active from passive nematics²⁵. The strength of the activity is set by ζ . The final term in equation (4) accounts for the friction, for example with a substrate, with γ the associated friction coefficient.

In a wet active nematic, the momentum propagation is more effectively suppressed as the friction coefficient is increased. In the limit of sufficiently high friction, the viscous and elastic stresses become small and the friction forces balance with the forces generated by the active term. In this regime the velocity can be approximated in terms of the nematic tensor as

$$u_i \approx -\frac{\zeta}{\gamma} \partial_j Q_{ij}. \quad (5)$$

Considering equation (5) as an equality and substituting in the equations (1-2) for the concentration and orientational order evolution, we reproduce the standard equations for dry active matter,

$$\partial_t \phi = \Gamma_\phi \nabla^2 \mu + \frac{\zeta \phi}{\gamma} \partial_i \partial_j Q_{ij} + \dots, \quad (6)$$

$$\partial_t Q_{ij} = \Gamma_Q H_{ij} + \dots. \quad (7)$$

The second term on the rhs of equation (6) is identical to that commonly introduced phenomenologically to represent the current due to curvature in the director field which drives ordering in dry active nematics. Thus, we demonstrate that the equations of dry active nematics can be generically reproduced from the nematohydrodynamic equations, showing that the dry limit arises naturally when friction dominates viscosity in wet active materials. We use $+\dots$ to denote that flow-driven terms which are non-linear in ϕ and Q also appear in this equation. We discuss these in the Supplementary Information and show that they can be derived from a kinetic approach introduced in¹⁹.

To demonstrate the wet to dry crossover, we present numerical solutions of the active nematic equations. We first illustrate the effect of increasing the friction on the evolution of the concentration and order parameter in a strongly ordered nematic (Fig. 2). Our dimensionless control parameter is $\eta\gamma/\zeta$, where η is the fluid viscosity.

Fig. 2a shows the time evolution of the concentration field (top row) and director field (bottom row) for an active nematic with an intermediate friction coefficient. As for zero-friction the nematic state is hydrodynamically unstable and walls form in the director field. However, both wall creation, and subsequent destruction by topological defects, are significantly slowed by the friction, which leads to a reduction in the RMS velocity field by a factor ~ 10 (Fig. 2c). Surprisingly, the slower dynamics is accompanied by an increase in the number of topological defects (Fig. 2d), a consequence of the larger number of walls at higher friction.

Linked to the wall formation is the emergence of coincident concentration bands, with a higher number of active particles at the walls, where the magnitude of the nematic ordering is reduced. The concentration ordering is driven by an advective flux of active particles towards the walls, down the gradient in \mathbf{Q} . In the steady state this is balanced by diffusion of the active particles from high to low concentrations.

Figs. 2c,d show that the active system behaves very differently for higher values of the friction. The RMS velocity is very low, and neither walls nor topological defects are formed. Fig. 2b indicates that concentration bands still appear in the dry limit but, in the absence of an advective flux, the way in which they are formed must be very different. The relevant mechanism is an instability driven by curvature in the nematic order, described by the final term in equation (6). The coupling between the concentration and the nematic order is established by the molecular potential resulting in a strong (weak) ordering at high (low) concentrations. Note the striking difference between the wet and dry limits: in the wet limit concentration bands are initially formed perpendicular to the director and concentration and nematic order are anticorrelated. In the dry limit the bands form parallel to the director and the concentration and nematic fields are correlated.

We next focus on the dynamical effects of friction at a temperature corresponding to the (passive) isotropic-nematic transition (Fig. 3). In a passive nematic there would be no orientational order. However in an extensile active system order is generated by the active forcing, and for the smallest value of friction considered, active turbulence is established. Flow vortices move around chaotically, decay and re-form (Fig. 3a). Positions of topological defects, are uncorrelated (Fig. 3d).

As the friction coefficient is increased there is a striking change in behaviour. As is apparent in Fig. 3b the velocity vortices form ordered, stationary arrays. The vortex sizes are consistent with a screening length for velocity propagation, $\sim \sqrt{\eta/\rho\gamma}$, which follows from the dissipation of activity-induced forces by a balance of viscosity and friction. At higher frictions Fig. 3c indicates how the vortices become narrower reflecting the decrease in the screening length.

The vortex-lattice is interleaved with an ordered network of topological defects (Figs. 3e,f). The defect lattice is a direct consequence of the velocity pattern: $+1/2$ defects are generated between pairs of counter-rotating vortices due to the change in the sign of the vorticity²¹, while $-1/2$ defects are created between two pairs of co-rotating vortices due to distinct flow-induced reorientation of nematic directors (Fig. 3g). The shear flow in the middle of a vortex turns a nematogen towards a 45 degree orientation relative to the vortex line, while extensional and compressional flows at the edges of a vortex induce vertical and horizontal reorientations, respectively.

Similar positional ordering of defects in equilibrium systems has been observed in Abrikosov lattices in type-II superconductors where magnetic fluxes are arranged in the form of small vortices²⁶. Recently, orientational, but not positional ordering of topological defects has been observed in experiments on microtubule bundles driven by molecular

motors²⁷ and it would be interesting to investigate further whether this too can be interpreted as a friction effect. Moreover it is noteworthy that the vorticity pattern we report at high friction resembles periodic vortex arrays reported recently for systems of particles with short range attractions²⁸ and vorticity patterns created by dividing cells²⁹.

Friction, with confining walls or between constituent active elements, is present in all active systems. Moreover friction can be tuned, providing mechanistic insights into pattern formation in active materials. For example, experiments on microtubules, actin filaments and cell cultures can probe the positional ordering of defects, predicted here, by varying the friction of active components with the substrate. The ability to control flow vorticity and defect structure will be important in the design and operation of biological and biomimetic materials. For example, one might envisage that such a vortex lattice has the potential to drive an array of microscopic gears. Here we have demonstrated that the balance between active and damping forces can drive the crossover between the characteristic dynamics of wet and dry active nematics, and identified a new phase of ordered velocity vortices and topological defects.

Methods

The governing equations of active nematohydrodynamics (equations (1)–(4)) describe a coupled system of partial differential equations. We employ a hybrid lattice Boltzmann technique to solve them. In this method, the equations describing the evolution of density and momentum (equations (3),(4)) are solved in tandem using a discretized version of the Boltzmann equation where the first and second moments of the particle distribution function give the density and momentum respectively. The BGK approximation with a single relaxation time is used in the collision operator. Equations (1),(2) which respectively describe the evo-

lution of the concentration and orientational order parameter are solved using the method of lines. All spatial differentials are discretised using the second order central difference scheme and time integration is performed using an Euler method. The time step for the method of lines is chosen as 1/10th of that for the lattice Boltzmann updates. The flow field used to evolve the order parameters is updated after every lattice Boltzmann time step while the active and passive stress are determined using the updated order parameter fields in every lattice Boltzmann step, hence ensuring the coupling between the equations in the algorithm. As usual in the lattice Boltzmann technique, discrete space and time steps are chosen as unity. Details can be found in^{23,30}. Simulations are performed on a 100×100 lattice. Unless otherwise stated, the parameters used are $\zeta = 0.008$, $\lambda = 0.7$, $\Gamma_\phi = 1.0$, $\Gamma_Q = 0.1$, $a = 0$, $A = -1.0$, $C = 0.6$, $K_\phi = 0.1$, $K_Q = 0.01$, $K_c = 0.0$, and $\eta = 0.05$, in lattice units.

Acknowledgements

We acknowledge funding from the ERC Advanced Grant MiCE. We thank Tyler Shendruk and Ramin Golestanian for helpful conversations.

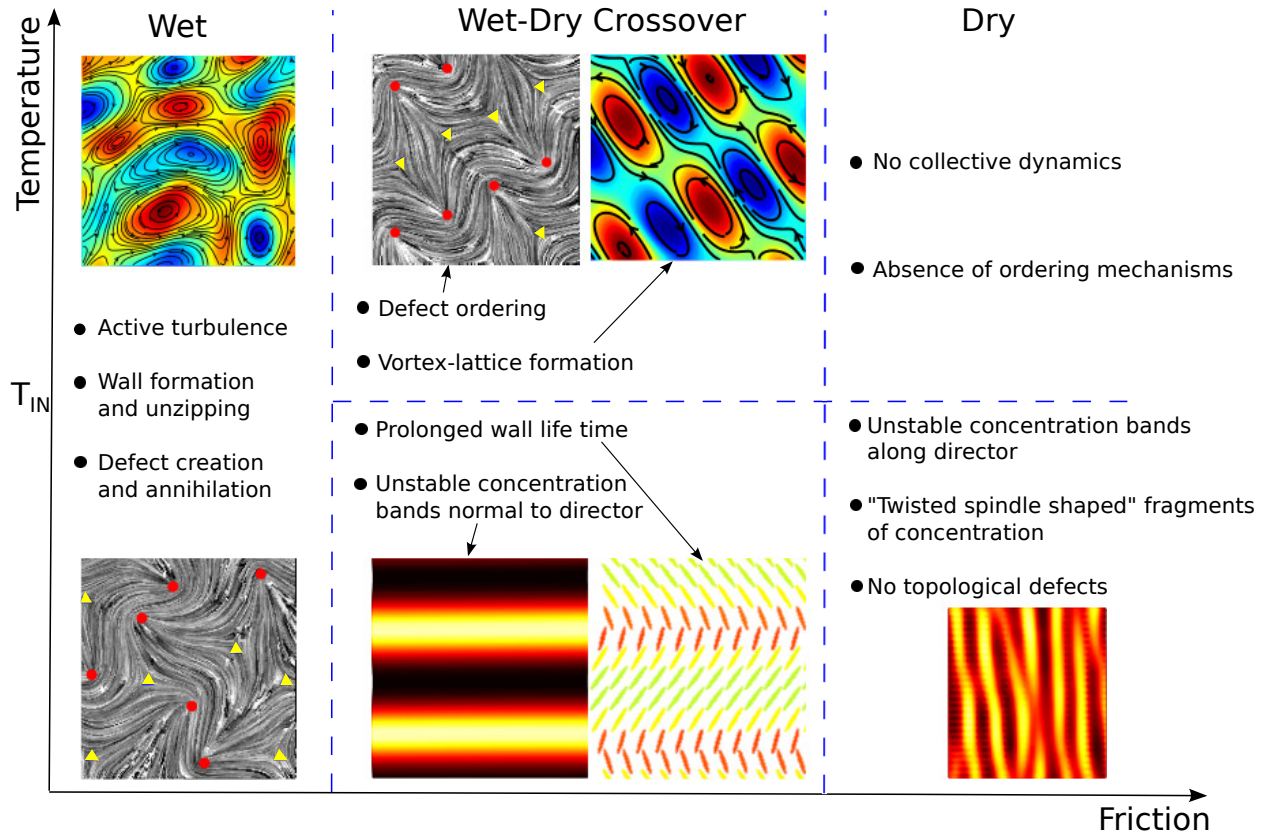


FIG. 1. Schematic representation of the wide range of dynamical behaviours of active nematics in the temperature-friction phase space. T_{IN} denotes the isotropic-nematic transition temperature: above T_{IN} at intermediate frictions we find a novel vortex lattice that entangles an ordered defect array. The blue-red colourmaps represent vorticity fields superimposed by streamlines (black solid lines). The concentration fields are depicted by red-yellow colourmaps. In the mid-lower section, the director field is illustrated by ellipsoids coloured by their orientations. Grey panels show director fields superimposed by topological defects (red circles and yellow triangles correspond to +1/2 and -1/2 defects).

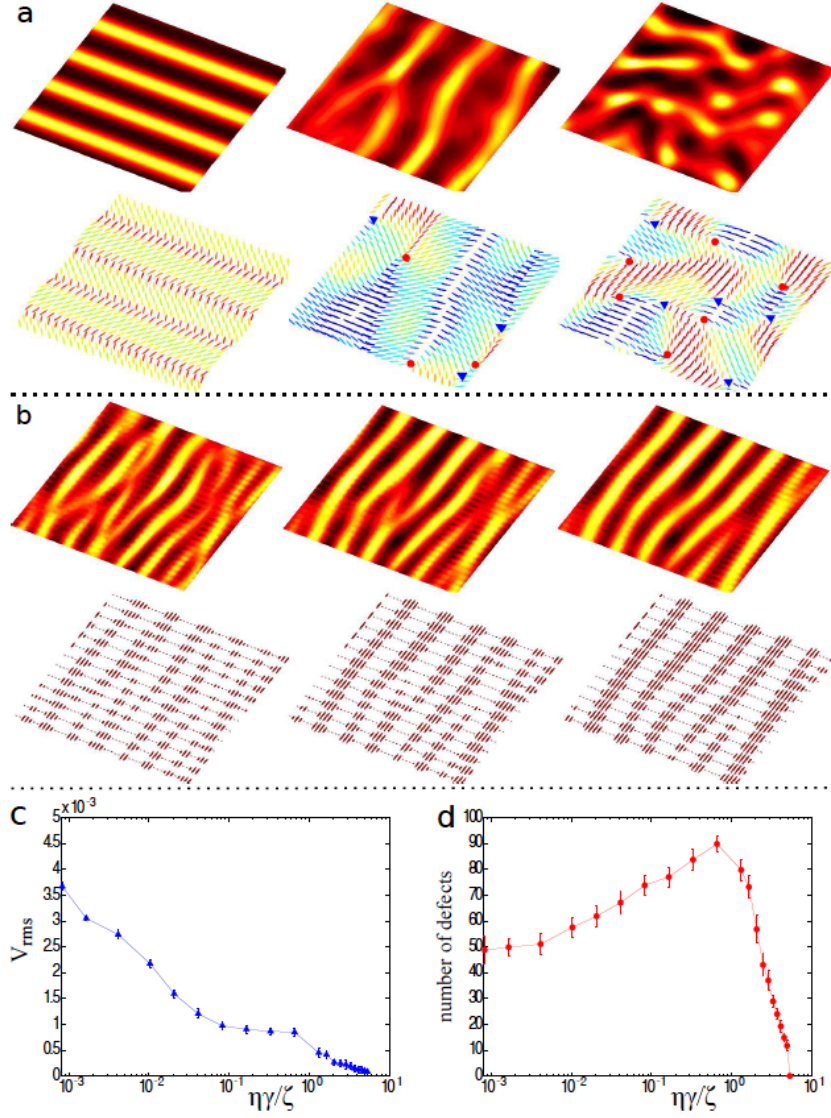


FIG. 2. Increasing friction drives the crossover from wet to dry active nematics. **a-b**, Temporal evolution of the concentration field and nematic director field for **a**, intermediate friction $\eta\gamma/\zeta = 1.88$, **b**, strong friction $\eta\gamma/\zeta = 5.36$. For each value of the friction the top row is a colour map indicating variations in concentration and the bottom row is the corresponding director field coloured by the orientation of nematic directors. The length of the major axis of each ellipsoid is proportional to the magnitude of its nematic order q . $+1/2$ and $-1/2$ defects are denoted by red circles and blue triangles. **c**, The RMS velocity is steadily reduced by increasing friction. **d**, The total number of topological defects initially increases, but drops sharply at $\eta\gamma/\zeta \sim 1$ and disappears at the dry limit.

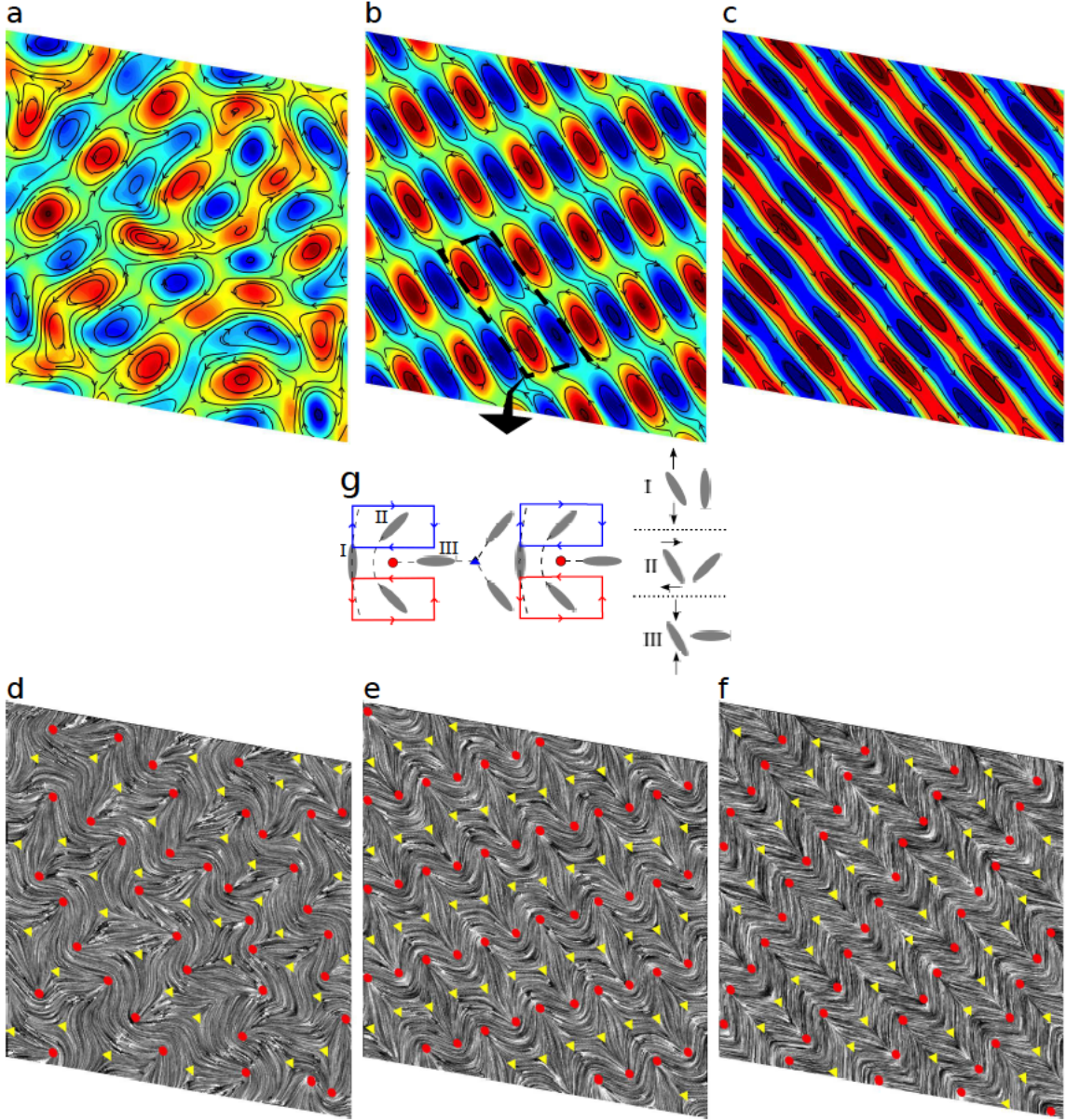


FIG. 3. **Emergence of a vortex-lattice and defect ordering with increasing friction.** **a-c**, Velocity field coloured by the magnitude of the vorticity. **d-f**, Director fields visualized by Line Integral Convolution and superimposed by topological defects (with $+1/2$ and $-1/2$ defects denoted by red circles and yellow triangles). The dimensionless friction is $\eta\gamma/\zeta=0.3, 0.6, 0.9$ for the left, middle, and right columns, respectively. **g**, Orientation of a defect is determined by its position relative to neighbouring vortices. A director responds differently to either extensional (I) or compressional (III) flow at the edges of vortices while it experiences a shear (II) inside a vortex.

REFERENCES

- ¹S. Ramaswamy, “The mechanics and statistics of active matter,” *Annu. Rev. Cond. Mat. Phys.* **1**, 323–345 (2010).
- ²D. L. Koch and G. Subramanian, “Collective hydrodynamics of swimming microorganisms: Living fluids,” *Annu. Rev. Fluid Mech.* **43**, 637–659 (2011).
- ³M. C. Marchetti, J. F. Joanny, S. Ramaswamy, T. B. Liverpool, J. Prost, M. Rao, and R. A. Simha, “Hydrodynamics of soft active matter,” *Rev. Mod. Phys.* **85**, 1143–1189 (2013).
- ⁴C. Dombrowski, L. Cisneros, S. Chatkaew, R. E. Goldstein, and J. O. Kessler, “Self-concentration and large-scale coherence in bacterial dynamics,” *Phys. Rev. Lett.* **93**, 098103 (2004).
- ⁵T. Sanchez, D. T. N. Chen, S. J. DeCamp, M. Heymann, and Z. Dogic, “Spontaneous motion in hierarchically assembled active matter,” *Nature* **491**, 431–434 (2012).
- ⁶Y. Sumino, K. H. Nagai, Y. Shitaka, D. Tanaka, K. Yoshikawa, H. Chate, and K. Oiwa, “Large-scale vortex lattice emerging from collectively moving microtubules,” *Nature* **483**, 448–452 (2012).
- ⁷V. Narayan, S. Ramaswamy, and N. Menon, “Long-lived giant number fluctuations in a swarming granular nematic,” *Science* **317**, 105–108 (2007).
- ⁸L. Giomi, M. J. Bowick, X. Ma, and M. C. Marchetti, “Defect annihilation and proliferation in active nematics,” *Phys. Rev. Lett.* **110**, 228101 (2013).
- ⁹F. C. Keber, E. Loiseau, T. Sanchez, S. J. DeCamp, L. Giomi, M. J. Bowick, M. C. Marchetti, Z. Dogic, and A. R. Bausch, “Topology and dynamics of active nematic vesicles,” *Science* **345**, 1135–1139 (2014).

- ¹⁰H. H. Wensink, J. Dunkel, S. Heidenreich, K. Drescher, R. E. Goldstein, H. Lowen, and J. M. Yeomans, “Meso-scale turbulence in living fluids,” *PNAS* **109**, 14308–14313 (2012).
- ¹¹J. Dunkel, S. Heidenreich, K. Drescher, H. H. Wensink, M. Bär, and R. E. Goldstein, “Fluid dynamics of bacterial turbulence,” *Phys. Rev. Lett.* **110**, 228102 (2013).
- ¹²A. Ward, F. Hilitski, W. Schwenger, D. Welch, A. W. C. Lau, V. Vitelli, L. Mahadevan, and Z. Dogic, “Solid friction between soft filaments,” *Nat. Mater.* (2015), [10.1038/nmat4222](https://doi.org/10.1038/nmat4222).
- ¹³S. K. Vedula, M. C. Leong, T. L. Lai, P. Hersen, A. J. Kabla, C. T. Lim, and B. Ladoux, “Emerging modes of collective cell migration induced by geometrical constraints,” *Proc. Nat. Acad. Sci.* **109**, 12974–12979 (2012).
- ¹⁴H. Gruler, U. Dewald, and M. Eberhardt, “Nematic liquid crystals formed by living amoeboid cells,” *EPJ B* **11**, 187–192 (1999).
- ¹⁵T. Vicsek and A. Zafeiris, “Collective motion,” *Phys. Rep.* **517**, 71–140 (2012).
- ¹⁶D. L. Blair, T. Neicu, and A. Kudrolli, “Vortices in vibrated granular rods,” *Phys. Rev. E* **67**, 031303 (2003).
- ¹⁷T. Vicsek, A. Czirók, E. Ben-Jacob, I. Cohen, and O. Shochet, “Novel type of phase transition in a system of self-driven particles,” *Phys. Rev. Lett.* **75**, 1226 (1995).
- ¹⁸E. Putzig and A. Baskaran, “Phase separation and emergent structures in an active nematic fluid,” *Phys. Rev. E* **90**, 042304 (2014).
- ¹⁹E. Bertin, H. Chaté, F. Ginelli, S. Mishra, A. Peshkov, and S. Ramaswamy, “Mesoscopic theory for fluctuating active nematics,” *New J. Phys.* **15**, 085032 (2013).
- ²⁰X. Shi, H. Chaté, and Y. Ma, “Instabilities and chaos in a kinetic equation for active nematics,” *New J. Phys.* **16**, 035003 (2014).
- ²¹S. P. Thampi, R. Golestanian, and J. M. Yeomans, “Velocity correlations in an active

- nematic,” *Phys. Rev. Lett.* **111**, 118101 (2013).
- ²²S. P. Thampi, R. Golestanian, and J. M. Yeomans, “Instabilities and topological defects in active nematics,” *Europhys. Lett.* **105**, 18001 (2014).
- ²³D. Marenduzzo, E. Orlandini, M. E. Cates, and J. M. Yeomans, “Steady-state hydrodynamic instabilities of active liquid crystals: Hybrid lattice Boltzmann simulations,” *Phys. Rev. E* **76**, 031921 (2007).
- ²⁴L. Giomi, L. Mahadevan, B. Chakraborty, and M. F. Hagan, “Excitable patterns in active nematics,” *Phys. Rev. Lett.* **106**, 218101 (2011).
- ²⁵R. A. Simha and S. Ramaswamy, “Hydrodynamic fluctuations and instabilities in ordered suspensions of self-propelled particles,” *Phys. Rev. Lett.* **89**, 058101 (2002).
- ²⁶E. H. Brandt, “The flux-line lattice in superconductors,” *Rep. Prog. Phys.* **58**, 1465 (1995).
- ²⁷S. J. DeCamp, G. S. Redner, A. Baskaran, M. Hagan, and Z. Dogic, “Orientational order of motile defects in active nematics,” (2015), [arXiv:1501.06228](https://arxiv.org/abs/1501.06228).
- ²⁸R. Großmann, P. Romanczuk, M. Bär, and L. Schimansky-Geier, “Vortex arrays and mesoscale turbulence of self-propelled particles,” *Phys. Rev. Lett.* **113**, 258104 (2014).
- ²⁹N. S. Rossen, J. M. Tarp, J. Mathiesen, M. H. Jensen, and L. B. Oddershede, “Long-range ordered vorticity patterns in living tissue induced by cell division,” *Nat. Commun.* **5** (2014), [10.1038/ncomms6720](https://doi.org/10.1038/ncomms6720).
- ³⁰S. P. Thampi, R. Golestanian, and J. M. Yeomans, “Vorticity, defects and correlations in active turbulence,” *Phil. Trans. R. Soc. A* **372**, 20130366 (2014).